International Journal of Naval Architecture and Ocean Engineering 12 (2020) 810–818

Contents lists available at ScienceDirect

International Journal of Naval Architecture and Ocean Engineering

journal homepage: http://www.journals.elsevier.com/international-journal-of-naval-architecture-and-ocean-engineering/

Estimation of damping induced by taut mooring lines

Lingzhi Xiong [a], Wenyue Lu [a, b, *], Xin Li [a, b], Xiaoxian Guo [a, b]

[a] State Key Laboratory of Ocean Engineering, Shanghai Jiao Tong University, 800 Dongchuan Road, Shanghai, 200240, China
[b] SJTU Yazhou Bay Institute of Deepsea Technology, Yonyou Media Center, No.5 Road, Yazhou District, Sanya, Hainan, 572000, China

ARTICLE INFO

Article history:
Received 8 July 2019
Received in revised form
14 November 2019
Accepted 19 December 2019
Available online 26 December 2019

Keywords:
Taut mooring line
Mooring line damping
Lumped mass method
Soil force

ABSTRACT

A moored floating structure may exhibit resonant motion responses to low-frequency excitations. Similar to the resonant responses of many vibration systems, the motion amplitude of a moored floating structure is significantly affected by the damping of the entire system. In such cases, the damping contributed by the mooring lines sometimes accounts for as much as 80% of the total damping. While the damping induced by catenary mooring lines is well-investigated, few studies have been conducted on the damping induced by taut mooring lines, especially one partly embedded in soil. The present study develops a simple but accurate model for estimating the damping contributed by mooring lines. A typical type of taut mooring line was used as the reference and the hydrodynamic drag force and soil resistance were taken into consideration. The proposed model was validated by comparing its predictions with those of a previously developed model and experimental measurements obtained by a physical model. Case studies and sensitivity studies were also conducted using the validated model. The damping induced by the soil resistance was found to be considerably smaller than the hydrodynamic damping. The superposition of the wave frequency motion on the low-frequency motion was also observed to significantly amplify the damping induced by the mooring lines.

1. Introduction

The mooring system is one of the key components of a moored floating structure, and may exhibit significant resonant responses to low-frequency excitations such as second-order wave forces. The maximum horizontal excursion of a mooring system is dominated by the second-order excitation force and the overall damping of the floating system, including the hull, mooring lines and risers (Brown et al., 1995). The damping contributed by mooring lines may account for up to 80% of the total damping for some floating systems (Huse and Matsumoto, 1989). The importance of considering the mooring line damping in the estimation of the slow drift motions of offshore floating facilities has been emphasized in various works (Brown and Mavrakos, 1999; Triantafyllou et al., 1994; Wichers and Huijsmans, 1990).

Mooring line damping was originally proposed by Huse (1986), who presented a simple numerical method for estimating the energy dissipation induced by the drag force on the mooring lines. Other related research tools have since been proposed, and these can be classified into three categories (Johanning et al., 2007): (a) simple analytical models, (b) fully dynamic finite element methods, and (c) physical model tests.

The original simple analytical model of Huse was improved by the superimposition of Wave Frequency (WF) motions on Low-Frequency (LF) motions (Huse and Matsumoto, 1989; Huse, 1991). The results showed that the combined WF and LF motions amplified the mooring line damping by a factor of 2–4. Liu and Bergdahl (1998) also improved Huse's original model by giving a new definition to the motion amplitude for energy dissipation integration. Bauduin and Naciri (2000) proposed a quasi-static model that enabled a more accurate prediction of the normal velocity of mooring line segments.

With regard to dynamic finite element methods, Webster (1995) proposed an indicator diagram method for estimating the mooring line damping. The mooring tension was particularly calculated by a fully dynamic finite element method. Yang et al. (2016) proposed a transformation method for obtaining the equivalent sinusoidal motion of a wave frequency random motion. The transformation was then used to estimate the mooring line damping due to the combined random LF and WF motions.

Huse and Masumoto (Huse and Matsumoto, 1988, 1989; Huse,

* Corresponding author.
E-mail address: lwy_qiye@sjtu.edu.cn (W. Lu).
Peer review under responsibility of Society of Naval Architects of Korea.

https://doi.org/10.1016/j.ijnaoe.2019.12.002

1986, 1991) performed experiments to determine the mooring line damping. Bauduin and Naciri (2000) also conducted decay tests on the surge motions of a mooring line to determine its damping. Another approach to accessing mooring line damping is the use of the indicator diagram method, which involves measurement of the load and displacement of the fairlead. Kitney and Brown (2001) experimentally investigated mooring line damping using large-scale (1:16) and small-scale (1:70) models. Johanning et al. (2007) observed an abrupt increase in the damping of a catenary mooring line after it was fully lifted, and thus highlighted a distinction between the damping characteristics of catenary and taut mooring lines.

Triantafyllou et al. (1994) noted the drag amplification caused by a vortex-induced vibration, and the possibility of it considerably increasing the mooring line damping. Nielsen and Bindingbø (2000) described the "drag locking" phenomenon, wherein the normal motion of the mooring line is restricted by significant drag forces. They derived the drag locking factor to estimate the mooring line damping. The majority of the above studies focused on catenary mooring lines, with only a few considering a taut mooring system, which is an attractive alternative to a catenary mooring system in deep water.

A taut mooring system requires an anchor with a large uplift load capacity, for which reason an embedded anchor is often used. The padeye of the embedded anchor is positioned at a certain depth beneath the mudline for the connection of the embedded mooring line. The design results in the soil resistance applying additional damping to the mooring system. This additional damping is different from the damping due to seabed friction and has not been previously investigated.

In the present study, a model was developed for prediction of the mooring line damping. The fully dynamic method was used to determine the mooring line responses. The following section introduces the theory for obtaining the mooring line dynamics and the damping coefficient. Section 3 describes the validation of the proposed model through comparison of its predictions with those of a previously developed model and the results of physical model tests. Section 4 presents some case studies that were used to investigate the damping of a typical taut mooring line through the imposition of different types of motions on the fairlead. The effect of the soil on the mooring line was considered. Section 5 describes a parametric study by which the sensitivity of the damping to the fairlead oscillation period and amplitude was examined. The patterns are summarised by using polynomial curves to fit the damping coefficient. In Section 6, some important conclusions drawn from the study are presented to afford better insight into the damping of the mooring line.

2. Theoretical background

2.1. Mooring line damping

The mooring line damping can be determined from the energy that is dissipated by the drag force and the soil resistance. The energy dissipation ΔE at an arbitrary segment during a cyclic period can be expressed as

$$\Delta E = \int_0^T \Delta \vec{F}\, d\vec{\eta} \tag{1}$$

where $\Delta \vec{F}$ denotes the drag force or soil resistance acting on the segment, $d\vec{\eta}$ is the displacement vector at the midpoint of the segment, and T is the period. Integrating Eq. (1) over the entire line gives the total energy E dissipated during a cycle.

The drag force $\Delta \vec{F}$ can be predicted using Morison's equation (Morison, 1950). It can be expressed as the sum of the normal and tangential contributions, for which the drag coefficients can differ by a factor of 20–50 (Palm, 2017).

$$\Delta \vec{F} = \frac{1}{2}\rho D(C_{dN}|V_N|V_N + C_{dT}|V_T|V_T)dl + \frac{1}{4}\rho\pi D^2 C_M \dot{V}^2 dl \tag{2}$$

where ρ is the water density, D is the nominal diameter of the segment, C_{dN} C_{dT}, and C_M are the drag coefficient in the normal direction, drag coefficient in the tangential direction, and mass coefficient, respectively, V and $\dot{V}$ are the relative velocity and acceleration at the midpoint of the segment, and dl is the segment length.

$\Delta \vec{F}$ or soil resistance is calculated using the equations of Neubecker and Randolph (1995):

$$\Delta \vec{F} = \vec{F}_l + \vec{Q} \tag{3}$$

$$\vec{F}_l = (E_\tau D f dl)\vec{\tau} \tag{4}$$

$$\vec{Q} = (E_n D q dl)\vec{n} \tag{5}$$

where $\vec{F_l}$ and $\vec{Q}$ are the tangential and normal components of the soil resistance, respectively. The bar diameter D is the same as that in Eq. (2). $\vec{\tau}$ and $\vec{n}$ are the unit vectors in the tangential and normal directions, respectively. In a dynamic analysis, $\vec{\tau}$ is assumed to be parallel to the line segment but opposite to the segment's tangential movement, and $\vec{n}$ is assumed to be opposite to the movement of the segment. E_τ and E_n are multipliers used to obtain the effective width of the mooring chain. The friction coefficient f and the averaged normal pressure q are obtained from the undrained shear strength S_u:

$$f = S_u \tag{6}$$

$$q = N_c S_u \tag{7}$$

$$S_u = S_{u0} - kz \tag{8}$$

where N_c is the bearing capacity factor for plane strain failure, assumed to be 7.6 in the present study; k is the gradient of the undrained shear strength; and z is the depth beneath the mudline (positive upward).

The accurate determination of the velocity in Eq. (2) is a key challenge. Some researchers have utilized simple analytical models with improved assumptions. In the present study, rather than attempting to estimate the normal velocity, we employed the instantaneous velocity and displacement of the line segment determined by dynamic simulation.

The mooring line dynamics has been well considered in numerous studies (Chen et al., 2001; Nakajima et al., 1982; Tahar et al., 2002), with the finite element method most widely used to tackle the problem. In this method, the mooring line is divided into several segments modelled by slender rod models (Garrett, 1982; Kim et al., 2005; Ran, 2000) or lumped mass models (Chai et al., 2002; Huang, 1994; Xiong et al., 2016a). The slender rod approach is particularly versatile for dealing with the complex boundaries, but it requires a good acquirement of mathematics. In the lumped mass approach, a line segment is assumed to consist of two lumped mass points connected by a massless spring. It is

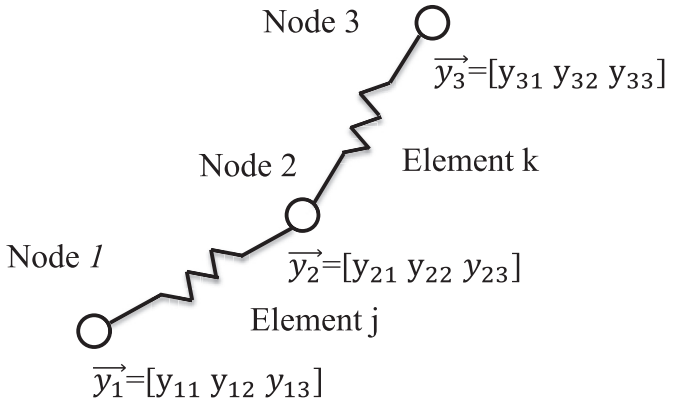

Fig. 1. Model for the lumped mass method.

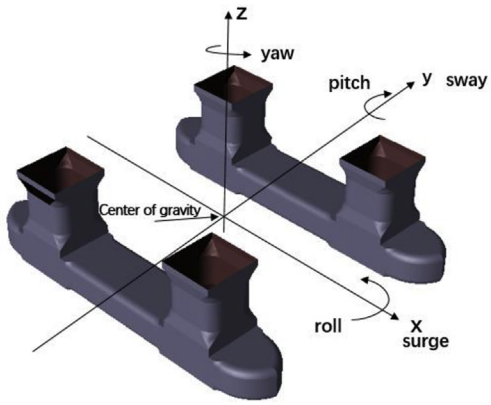

Fig. 2. The sketch of the motion definition.

numerically more efficient and has a clear physical meaning, which facilitates the incorporation of the soil resistance. The lumped mass approach was adopted in the present study.

2.2. Lumped mass method

As shown in Fig. 1, the profile of a mooring line can be represented by lumped mass segments. In the figure, the nodes are arbitrarily numbered from 1 to 3 and connected by elements j and k. The coordinates of the nodes are represented by $\overrightarrow{y_1}$, $\overrightarrow{y_2}$, $\overrightarrow{y_3}$ respectively. The application of Newton's second law to each node along the line yields

$$M\ddot{y} = F \tag{9}$$

where M is the node mass, including the added mass, and F is the external force acting on the node, including the elastic tension from the two adjacent elements, wet weight, hydrodynamic loads, and soil resistance. Each segment is divided into two halves. The properties (mass, length, drag force, etc.) of each half are lumped and assigned to the adjacent node. All the components of the external forces and the solution strategy are discussed with more detail by Xiong et al. (2016a).

2.3. Linear damping coefficient

Assuming the occurrence of forced sinusoidal oscillations of the fairlead in the X or Z direction, given by

$$X = A_{LF}\sin\left[2\pi\left(\frac{t}{T_{LF}}\right)\right] + A_{WF}\sin\left[2\pi\left(\frac{t}{T_{WF}}\right)\right] \tag{10}$$

$$Z = Z_{amp}\sin\left[2\pi\left(\frac{t}{T_{heave}}\right)\right] \tag{11}$$

where A_{LF}, A_{WF}, and Z_{amp} are respectively the oscillatory amplitudes of the LF and WF surge motions and the heave motion, and T_{LF}, T_{WF}, and T_{heave} are the corresponding oscillation periods. The definitions of the motions are presented in Fig. 2.

The component of the tension in the X direction, F_x, can be expressed in terms of the equivalent linear damping B_d, as follows:

$$F_x = B_d\frac{dX}{dt} \tag{12}$$

In addition, the dissipated energy can be estimated by the indicator diagram method using the following equation (Brown and Mavrakos, 1999):

$$E = \int_0^\tau F_x\frac{dX}{dt}dt = \int_0^\tau B_d\left(\frac{dX}{dt}\right)^2 dt \tag{13}$$

Because the mooring line damping is believed to be affected mainly by the LF motion, only the LF excitation was considered in the item dX in the present study. The upper limit of integration τ was set to be the period of the LF motion (Brown and Mavrakos, 1999; Yang et al., 2016; Qiao and Ou, 2014).

The equivalent linear damping coefficient was thus obtained as

$$B_d = \frac{BT_{LF}}{2\pi^2 A_{LF}^2} \tag{14}$$

3. Validation

The proposed model was validated by comparing its predictions with those of a previously developed model and the results of physical model tests.

3.1. Validation against physical model tests

Decay tests were conducted in calm water to measure the damping of a mooring system designed for the semi-submersible shown in Fig. 3. The tests were conducted at Shanghai Jiao Tong University. The water depth was 600 m and the parameters of the mooring system were as detailed in Table 1. The detailed experimental set-up was summarised in the previous study (Xiong et al., 2016b). The decay tests were initially conducted with the semi-

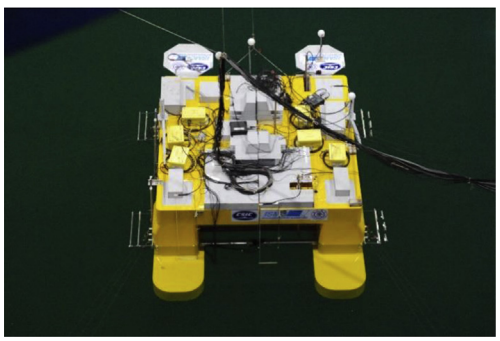

Fig. 3. Semi-submersible in the calm water of a wave basin.

Table 1
Properties of the line mooring system.

Segment	Length (m)	Diameter (mm)	Net Weight (N/m)	EA (MN)	Pretension (kN)
Upper Chain	450	105	1871.75	940.99	2000
Middle Section (Wire rope)	478.6	190	735.65	63.52	
Seabed Chain	425.0	105	2174.98	58.81	

Notes
1. Distance between anchor point and fairlead = 1175 m
2. Distance between touch down point and fairlead = 952.4 m
3. Horizontal pretension = 905 kN

submersible moored by four horizontal mooring lines, which were set just above the water surface. The measured damping coefficients represented the viscous and radiation damping of the vessel model. The four horizontal mooring lines were subsequently replaced by a truncated mooring system and the tests were repeated to determine the total damping of the vessel and mooring system. The damping of the mooring system could thus be obtained. The decay curves of the surge motions during the tests are shown in Fig. 4.

Table 2 presents the damping of the mooring line obtained by the surge decay tests and the proposed method. In the numerical simulation, the LF surge amplitude under the survival condition (25.6 m) was adopted as the amplitude of the imposed sinusoidal oscillation of the fairlead. It was determined by low-pass filter (filtering frequency = 0.2 rad/s) processing of the surge time series under the survival condition in a fully coupled dynamic analysis. The natural period (200 s) was set as the oscillation period. The comparison of the test and numerical results in Table 2 reveals good agreement.

3.2. Verification with a previous study

Bauduin and Naciri (2000) (henceforth referred to as B&N) introduced two types of mooring lines that represented typical mooring lines used in shallow and deep waters, respectively (see Table 3 for details). In their study, they imposed several X-direction mono-frequency sinusoidal oscillations on the fairlead. The details of the oscillations and the damping of the mooring lines estimated

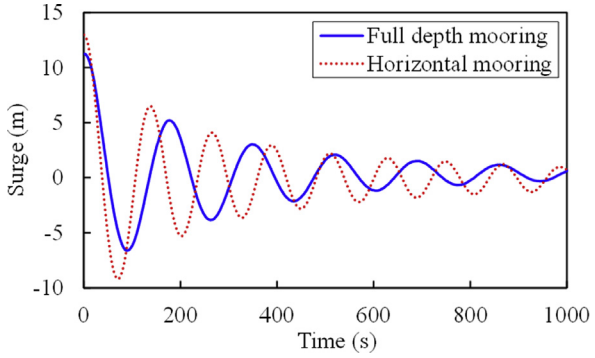

Fig. 4. Decay curves of the surge motions for two different mooring systems: horizontal mooring system and full-depth mooring system.

Table 2
Damping determined by model decay tests and the proposed method.

Model Test			Proposed Method	Deviation
Mooring and hull	Hull only	Mooring	Mooring	
490.7 MJ	165.9 MJ	324.8 MJ	307.3 MJ	5.4%

Table 3
Properties of the mooring line used for the validation (B&N).

	Line 1	Line 2
Water depth (m)	82.5	500
Unstretched total length (m)	711.3	4000
Line type	Chain	Wire
Diameter (mm)	140	130
Normal drag coefficient	3.2	1.8
Weight in air (N/m)	3586.5	800.5
Weight in water (N/m)	3202.0	664.4
Axial stiffness EA (N)	1.69E9	1.30E9
Horizontal pretension (kN)	427.7	1905.3
Pretension angle (deg)	51.8	31.6
Anchor fairlead distance (m)	683.4	3910.1
Anchor lift-fairlead distance (m)	541.6	2239.1

in their study and other previous studies (Huse, 1991; Liu and Bergdahl, 1998), as well as the estimations obtained by the present model, are presented in Table 4 and Table 5. The last columns of the tables give the relative error between the results of the present study and those of B&N.

The energy dissipation of Line 1 and Line 2 are listed in Tables 4 and 5, respectively. The deviation is obtained by comparing the present results with those of B&N results. The deviation results show good agreement between the present results and those of B&N. The present Line 2 results are slightly larger than those of B&N because the latter included only the normal component of the mooring line displacement and ignored the tangential component. The present study naturally considers both components (see Eq. (1)). The deviation was observed due to the effect of the interactions between mooring lines and the soil was taken into consideration in the proposed method in the present study.

Table 4
Dissipated energy of Line 1 (unit: MJ).

Excitation	Huse (Huse, 1991)	Liu (Liu and Bergdahl, 1998)	B&N	Proposed	Deviation
5.4 m, 10 s	3.670	4.190	4.466	4.701	5.26%
10 m, 100 s	0.247	0.360	0.365	0.381	4.38%
20 m, 100 s	2.700	6.730	8.100	7.931	−2.09%
10 m, 200 s	0.062	0.090	0.089	0.092	3.37%
20 m, 200 s	0.675	1.680	2.005	2.010	0.25%

Table 5
Dissipated energy of Line 2 (unit: MJ).

Excitation	Huse (Huse, 1991)	Liu (Liu and Bergdahl, 1998)	B&N	Present	Deviation
5.4 m, 10 s	150.05	151.12	143.90	149.329	3.77%
30 m, 330 s	20.84	24.07	24.24	25.158	3.79%
50 m, 330 s	85.19	117.38	123.50	131.62	6.57%

Table 6
Properties of the taut mooring line.

	Length (m)	Diameter (mm)	Wet weight (N/m)	EA (MN)	Drag Coefficient C_d^n
Ground chain	100	127	3335.4	1540	2.4
Mid-section (polyester)	700	201	71.6	267	1.8
Upper chain	65	127	3335.4	1540	2.4

Notes
1. water depth = 500 m; 2. embedded depth of the padeye = 20 m
3. $E_\tau = 8.0$, $E_n = 2.5$, and $N_c = 7.6$

4. Case study

A three-component, taut mooring line with the properties given in Table 6 was considered. The upper and lower components of the line consisted of chains, while the middle component was made from polyester. The axial stiffness of the polyester was assumed to be constant. The model of the line is shown in Fig. 5. The water depth was 500 m, the embedded depth of the padeye was 20 m, and the undrained shear strength of the soil was determined using $S_u = 1.5z\ kPa$ (Andersen et al., 2005). The parameters E_τ, E_n and N_c were 8.0, 2.5, and 7.6, respectively. Considering the complex motion of an offshore floating platform, different types of motions were imposed on the fairlead, e.g., LF motion only, WF motion only, and a combination of both, as detailed in Table 7. A period of 15 s was applied to the WF motion, because waves with periods on this order are common in open seas. The period of 150 s applied to the LF motion is the typical natural period of the surge/sway motion of a moored offshore floating structure. The soil effect was particularly not considered in Cases X5-X8 to demonstrate the influence of the soil.

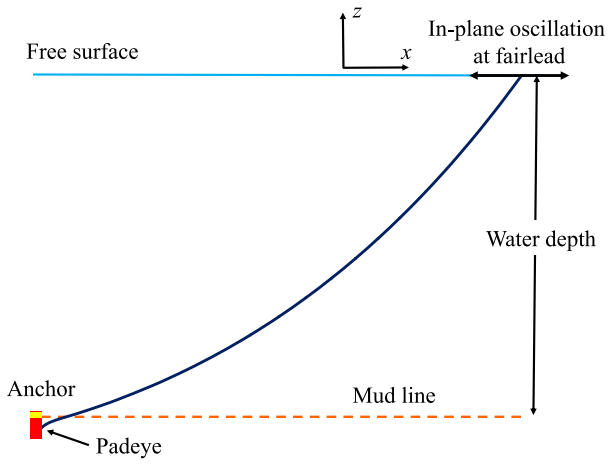

Fig. 5. Set-up of the mooring line for the simulation.

Case X8 represented a combination of the LF case (X5) and WF case (X6). The hydrodynamic damping in Case X8 was greater than those in Cases X5 and Case X6, and even exceeded the summation of the two. Huse and Matsumoto (1989) noted that the superposition of a WF motion on an LF motion could amplify the damping of a catenary mooring line by a factor of 2–4. However, in the case of the present taut mooring line, some of the damping amplification factors were much higher. For example, the energy dissipated during a cycle in Case X8 (14.05 MJ) was more than 12 times that of Case X6 (1.17 MJ), and 25 times that of Case X5 (0.56 MJ). This indicates that wave frequency motions are important for the system's generation and amplification. It should also be noted that the mooring line-induced damping is a low-frequency item that is mainly induced by the low-frequency motion. Moreover, the mooring-induced damping mainly affects the low-frequency motion. Johanning et al. (2007) observed that when a line is taut, a small movement at the fairlead produced very large perpendicular movements or velocities in the suspended mooring line. Given that the drag force that generates the damping is proportional to the square of the velocity, a small increase in the movement speed at the fairlead would result in considerable energy dissipation. This is because the superposition of a WF motion significantly amplifies the velocity of the mooring line, leading to a substantial increase in the damping.

Although Cases X7 and X8 had identical maximum excursions at the fairlead, and the same excitation period, the damping in Case X8 was significantly greater. The discrepancy was obviously due to the imposed WF motion in Case 8, which increased the mooring line velocity, resulting in a greater drag force on the mooring line. An analogous conclusion can be drawn from a comparison of the hydrodynamic damping of Cases X1-X4. Interestingly, the hydrodynamic damping of the LF motion cases was slightly lower when the soil effect was considered (Cases X2 and X3). In contrast, the hydrodynamic damping of the WF motion cases without consideration of the soil effect (X5 and X8) was much higher than those of the cases in which the soil effect was considered (X1 and X4). This was because the soil effect reduced the length of the mooring line in the water and restricted the motion of the suspended component. It is thus obvious that consideration of the soil damping increases the total damping. However, in the cases of only WF motion, the total damping when the soil effect was considered was still lower than that when the effect was not considered. This was because the soil damping accounted for less than 16% of the total damping.

The soil damping was significantly less than the hydrodynamic damping in Cases X1-X4, because the length of the mooring line in the soil was much shorter than that in the water. The soil damping in Case X4 was greater than the summation of those of Cases X1 and X2, indicating that the superimposition of the WF motion significantly increased the soil damping. However, the hydrodynamic

Table 7
X-direction oscillation case matrix (damping unit: kNs/m).

Case	Amplitude (m)	Period (s)	Hydrodynamic Damping	Dissipated Energy (Hydro-dynamic) (MJ)	Soil damping	Total damping	Notes
X1	5	15	8.6	0.28	2.3	10.8	With soil
X2	15	150	36.9	1.09	23.0	59.8	
X3	20	150	45.0	2.37	18.0	63.0	
X4	X1+X2		323.8	9.59	61.0	384.8	
X5	5	15	17.0	0.56	–	17.0	No soil
X6	15	150	39.5	1.17	–	39.5	
X7	20	150	48.1	2.54	–	48.1	
X8	X5+X6		474.5	14.05	–	439.5	

damping remained the predominant source of damping.

5. Parameter sensitivity study

A parameter sensitivity study was conducted to investigate the effect of the oscillation amplitude and period on the damping coefficient. The mooring line configuration used for this investigation was the same as that in Section 4. The case matrixes are presented in Table 8 and Table 9. The considered periods of the WF motion were within 10–30 s, while those of the LF motion were within 50–200 s.

5.1. Effect of oscillation period on the damping coefficient

The effect of the oscillation period at the fairlead was investigated. Fig. 6 shows the damping coefficient with respect to the oscillation period. The results for cases of only WF motion are shown in Fig. 6 (a), which reveals that the hydrodynamic damping decreases with increasing oscillation period, while the soil damping increases. This is attributable to the high velocity of the suspended line and the resultant large drag force for a short oscillation period. Conversely, the motion of an embedded anchor chain tends to be affected by a long-period excitation, resulting in more energy being dissipated and a large soil damping. In such cases in the present study, namely, Cases A5-A8, which involved only LF motions, the soil damping increased with increasing oscillation period. However, the trend of the hydrodynamic damping was more complex, with the soil damping slightly increasing with increasing period from 50 to 150 s, and thereafter decreasing (see Fig. 6 (b)).

Fig. 6 (c) shows the effect of the WF motion period in the bi-harmonic excitation (superimposition of WF and LF motions). It can be observed from the figure that both the hydrodynamic and soil damping decrease with increasing period of the WF motion, with the decrease of the hydrodynamic damping being more significant. Conversely, Fig. 6 (d) shows that the two damping increase with increasing period of the LF portion of the bi-harmonic motion. This is due to the increasing number of WF cycles during one LF period with increasing oscillation period, resulting in substantial amplification of the damping.

In summary, the damping coefficient complexly fluctuates with the variation of the oscillation periods. The hydrodynamic damping decreases with increasing period of the WF motion, for both mono-harmonic and bi-harmonic excitations. The reverse is, however, the case in the presence of soil damping, with the exception of when

Table 8
Case matrix for oscillations in the X-direction only.

Surge Only	Wave Frequency		Low Frequency		Hydrodynamic Damping (kNs/m)	Soil Damping (kNs/m)	Total Damping (kNs/m)
	Amplitude (m)	Period (s)	Amplitude (m)	Period (s)			
A1	5	10	–	–	11.1	1.6	12.7
A2	5	15	–	–	8.6	2.3	10.8
A3	5	20	–	–	7.7	3.0	10.7
A4	5	30	–	–	6.9	4.3	11.2
A5	–	–	20	50	32.7	6.8	39.5
A6	–	–	20	100	43.3	12.6	55.9
A7	–	–	20	150	45.0	18.0	63.0
A8	–	–	20	200	41.8	22.9	64.7
B1	8	15	–	–	15.5	2.8	18.2
B2	10	15	–	–	19.8	2.9	22.7
B3	12	15	–	–	23.4	3.0	26.4
B4	14	15	–	–	26.0	3.8	29.8
C1	5	10	15	150	687.1	87.7	774.8
C2	5	15	15	150	323.8	61.0	384.8
C3	5	30	15	150	113.0	37.2	150.3
C4	2	15	15	150	81.0	30.6	111.5
C5	4	15	15	150	216.7	48.5	265.1
C6	6	15	15	150	458.0	75.2	533.2
C7	5	10	15	50	110.1	15.3	125.4
C8	5	10	15	100	336.5	44.5	381.1
C9	5	10	15	200	1173.2	145.8	1319.0

Table 9
Case matrix for oscillations in the X-Z plane.

Surge + Heave	*X* direction		*Z* direction		Hydrodynamic Damping (kNs/m)	Soil Damping (kNs/m)	Total Damping (kNs/m)
	Amplitude (m)	Period (s)	Amplitude (m)	Period (s)			
D1	–	–	5	15	36.2	1.1	37.3
D2	–	–	8	15	41.8	1.3	43.1
D3	–	–	10	15	45.5	1.5	47.0
D4	–	–	12	15	49.0	1.7	50.7
E1	5	15	5	15	63.3	9.1	72.5
E2	5	15	8	15	158.8	16.1	174.9
E3	5	15	10	15	245.8	28.4	274.2
E4	5	15	12	15	346.5	45.3	391.8
E5	20	150	5	15	362.3	34.9	397.2
E6	20	150	8	15	925.5	67.6	993.0
E7	20	150	10	15	1440.4	136.6	1577.0
E8	20	150	12	15	2078.2	211.1	2289.3

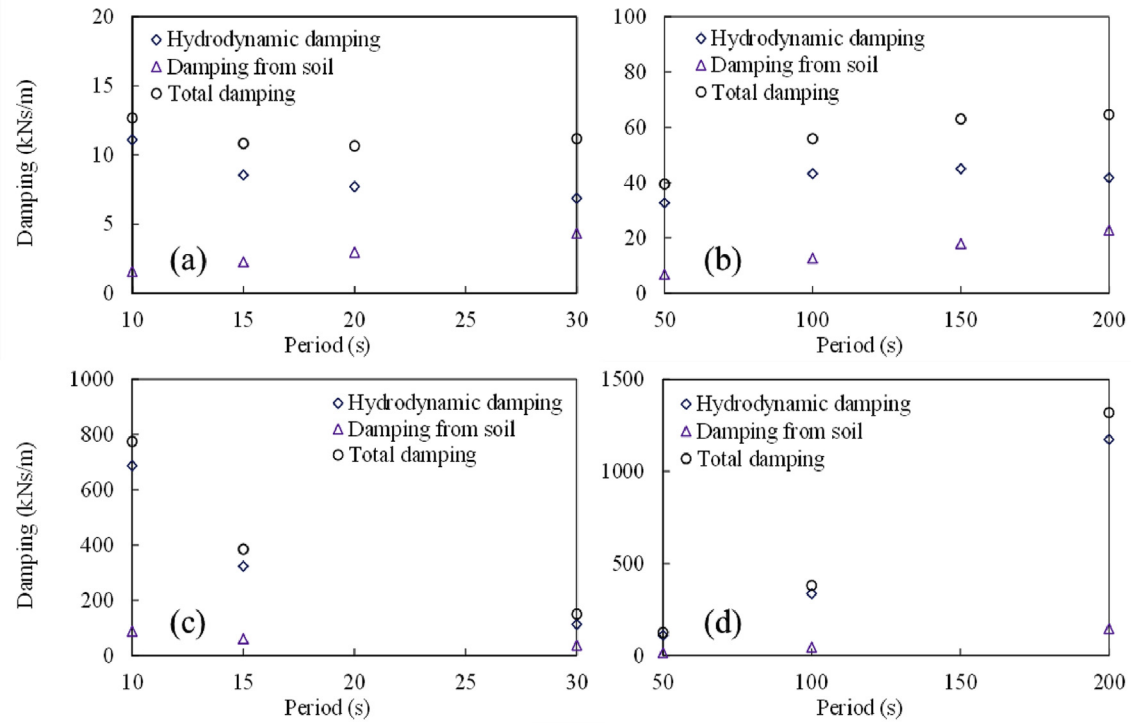

Fig. 6. Effect of the oscillation period on the damping coefficient: (a) WF surge motion only (Cases A1-A4), (b) LF surge motion only (Cases A5-A8), (c) Fixed LF motion combined with WF motion of varying period (Cases C1–C3), and (d) Fixed WF motion combined with LF motion of varying period (Cases C7–C9).

the increase of the WF motion period occurs alongside a fixed LF motion period.

5.2. Effect of the motion amplitude on the damping coefficient

The observed effect of the oscillation amplitude on the damping coefficient is shown in Fig. 7. As indicated, the two types of damping increase with increasing oscillation amplitude of the WF motion (under both mono-harmonic and bi-harmonic conditions). This is obviously due to the increase in the drag force with increasing oscillation amplitude of the fairlead.

5.3. Effect of vertical motions on the damping coefficient

In the preceding sections, only the X-direction oscillations were considered. In reality, an offshore platform undergoes significant movements in the vertical plane in a complex metocean scenario. Consequently, the Z-direction oscillation (heave motion) was also considered in the present study to investigate the effect of vertical motion on the damping. The oscillation period was fixed to 15 s, while the amplitude was varied within 5–12 m. The considered cases comprised three categories, namely, heave motion only, heave motion combined with WF motion in the X-direction, and heave motion combined with LF motion in the X-direction. The phases of the surge motion relative to the heave motion are zero.

The results of the tests are presented in Table 9 and Fig. 8. As can be observed, in the cases of only heave motion, the hydrodynamic damping is the predominant component of the total damping, with soil damping contributing only 3%. However, both damping types increase with increasing oscillation amplitude, as shown in

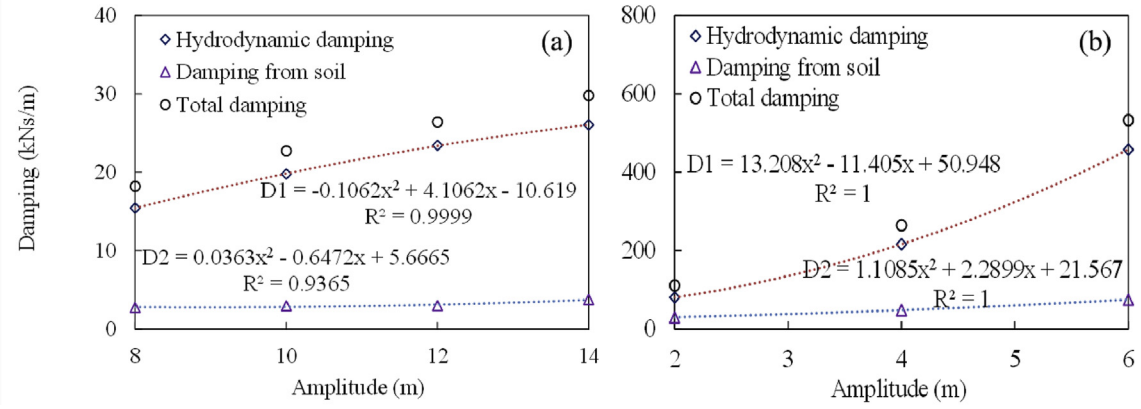

Fig. 7. Effect of the oscillation amplitude on the damping coefficient: (a) WF motion only (Cases B1–B4), and (b) fixed LF motion combined with WF motion of varying amplitude (Case C4–C6). (R is the coefficient of correlation or fitting degree.)

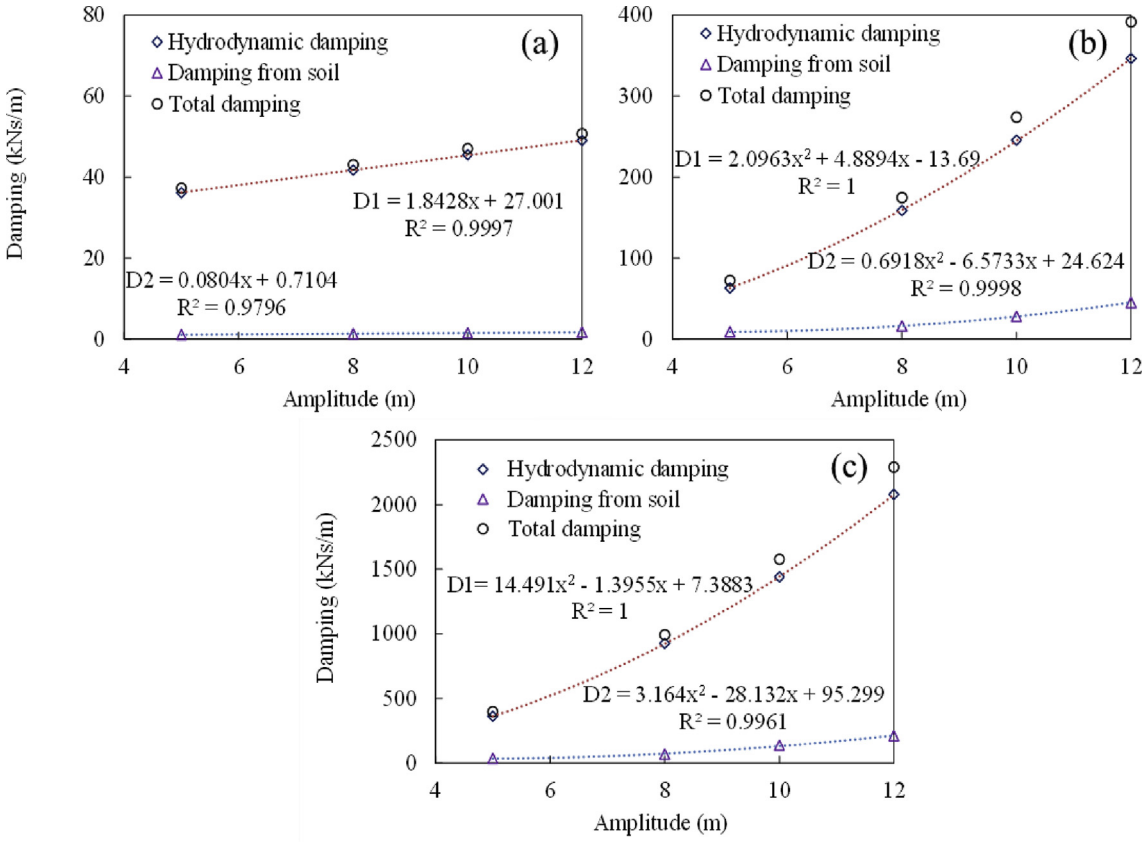

Fig. 8. Effect of Z-direction oscillation on the damping coefficient: (a) heave motion only (Cases D1-D4), (b) heave motion combined with WF motion in the X-direction (Cases E1-E4), and (c) heave motion combined with LF motion in the X-direction (Cases E5-E8). (R is the coefficient of correlation or fitting degree.)

Fig. 8(a). In Fig. 8(b) and (c), which correspond to fairlead motions in the X- and Z-directions, the hydrodynamic damping is notably amplified with increasing amplitudes of both motions. The soil damping also increases with increasing amplitude of the heave motion, with the proportion of the soil damping also increasing to 12.6% of the total damping.

To clarify the effect of the heave motion, Cases E1-E4 were compared with Case A2, and Cases E5-E8 with B7. It is notable that the superimposition of the heave oscillation significantly increased the two types of damping. If the two type of damping in Cases D1-D4 are respectively added to those in Cases A2 and B7, the damping would still be much smaller than those of Cases E1-E8. This is because the tension in the mooring line significantly fluctuates with the X-direction oscillation of the fairlead. Webster (1995) observed that the hydrodynamic damping behavior of the mooring line varied with the tension. The resultant hydrodynamic damping under combined the X- and Z-direction motions would thus differ from the simple summation of the damping under only the X-direction motion and only the Z-direction motion, respectively. An analysis of the results regarding the soil damping reveals that it is more significantly affected by the X-direction motion, especially the LF motion, than the Z-direction motion.

6. Conclusions

The damping characteristic of a taut mooring line was investigated. The energy dissipation during the dynamic mooring process was used to evaluate the damping. In addition to the hydrodynamic damping, the damping produced by the soil resistance was also investigated to examine its impact on the taut mooring line. In the tests, the mooring nine was excited through the application of forced sinusoidal oscillations to the fairlead. Some useful conclusions drawn from the findings of the study are as follows:

The damping contributed by the soil resistance is substantially smaller than the hydrodynamic damping, owing to the relatively short embedded length of the anchor chain. The total damping for cases with soil damping is less than that for cases without soil damping, with the exception of when there is only LF motion.

The presence of soil damping reduces the hydrodynamic damping. There are two possible reasons for the reduction of the hydrodynamic damping: (1) the reduced length of the mooring line in water, and (2) the force exerted by the soil on the line restricts the motion of the mooring line to some extent.

The increase in the damping of the taut mooring line resulting from the imposition of the WF motion is significantly larger than that for a catenary mooring line. This indicates that wave frequency motions are important for the generation and amplification to system. A possible reason for this is the proportionality of the drag force to the square of the velocity, which can be reflected in the Morrison's method. For the taut mooring line, small increases in the motion speed and amplitude at the fairlead would cause a considerable increase in the drag force on the entire line, resulting in a significant increase in the damping. This may be advantageous to the mooring line tensions, otherwise the tensions would be increase distinctly with slightly growing motions.

The hydrodynamic damping increases dramatically with increasing motion amplitude in the X-direction.

The soil damping is affected more by an X-direction motion than by a Z-direction motion.

The hydrodynamic and soil damping increase with increasing

motion in the Z-direction, as does the proportion of soil damping with increasing amplitude of the Z-direction motion.

Acknowledgements

This work was financially supported by the National Natural Science Foundation of China (Grant no. 51709169) and the open foundation of State Key Laboratory of Ocean Engineering (Shanghai Jiao Tong University) (Grant No. 1618).

References

Andersen, K., Murff, J., Randolph, M., Clukey, E., Erbrich, C., Jostad, H., Hansen, B., Aubeny, C., Sharma, P., Supachawarote, C., 2005. Suction anchors for deepwater applications. In: Proceedings of the International Symposium on Frontiers in Offshore Geotechnics (ISFOG), pp. 3–30.

Bauduin, C., Naciri, M., 2000. A contribution on quasi-static mooring line damping. J. Offshore Mech. Arct. Eng. 122, 125.

Brown, D., Mavrakos, S., 1999. Comparative study on mooring line dynamic loading. Mar. Struct. 12 (3), 131–151.

Brown, D., Lyons, G., Ln, H., 1995. Advances in mooring line damping. Underw. Technol.: Int. J. Soc. Underw. 21 (2), 5–11.

Chai, Y., Varyani, K., Barltrop, N., 2002. Three-dimensional lump-mass formulation of a catenary riser with bending, torsion and irregular seabed interaction effect. Ocean Eng. 29 (12), 1503–1525.

Chen, X., Zhang, J., Ma, W., 2001. On dynamic coupling effects between a spar and its mooring lines. Ocean Eng. 28 (7), 863–887.

Garrett, D., 1982. Dynamic analysis of slender rods. J. Energy Resour. Technol. 104 (4), 302–306.

Huang, S., 1994. Dynamic analysis of three-dimensional marine cables. Ocean Eng. 21 (6), 587–605.

Huse, E., 1986. Influence of mooring line damping upon rig motions, offshore Technology conference. In: Offshore Technology Conference.

Huse, E., 1991. New developments in prediction of mooring line damping. In: 23th Offshore Technology Conference. OTC, pp. 6–9.

Huse, E., Matsumoto, K., 1988. Practical estimation of mooring line damping. In: Offshore Technology Conference.

Huse, E., Matsumoto, K., 1989. Mooring line damping due to first- and second-order vessel motion. In: Offshore Technology Conference, pp. 135–148.

Johanning, L., Smith, G.H., Wolfram, J., 2007. Measurements of static and dynamic mooring line damping and their importance for floating WEC devices. Ocean Eng. 34 (14), 1918–1934.

Kim, M., Koo, B., Mercier, R., Ward, E., 2005. Vessel/mooring/riser coupled dynamic analysis of a turret-moored FPSO compared with OTRC experiment. Ocean Eng. 32 (14), 1780–1802.

Kitney, N., Brown, D., 2001. Experimental investigation of mooring line loading using large and small-scale models. J. Offshore Mech. Arct. Eng. 123 (1), 1–9.

Liu, Y., Bergdahl, L., 1998. Improvements on huse's model for estimating mooring cable induced damping. In: 17th International Conference on Offshore Mechanics and Arctic Engineering.

Morison, J.R., 1950. The Force Exerted by Surface Waves on Piles. Pet. Trans., AIME.

Nakajima, T., Motora, S., Fujino, M., 1982. On the dynamic analysis of multi-component mooring lines. In: Offshore Technology Conference.

Neubecker, S., Randolph, M., 1995. Profile and frictional capacity of embedded anchor chains. J. Geotech. Eng. 121 (11), 797–803.

Nielsen, F.G., Bindingbø, A.U., 2000. Extreme loads in taut mooring lines and mooring line induced damping: an asymptotic approach. Appl. Ocean Res. 22 (2), 103–118.

Palm, Johannes, 2017. Mooring Dynamics for Wave Energy Applications. Diss. PhD thesis. Chalmers University of Technology.

Qiao, D., Ou, J., 2014. Mooring line damping estimation for a floating wind turbine. Sci. World J.

Ran, Z., 2000. Coupled Analysis of Floating Structures in Waves and Currents. Texas A&M University.

Tahar, A., Ran, Z., Kim, M., 2002. Hull/mooring/Riser coupled spar motion analysis with buoyancy-can effect. In: Proceedings of the 12th International Offshore and Polar Engineering Conference.

Triantafyllou, M., Yue, D., Tein, D., 1994. Damping of moored floating structures. In: Offshore Technology Conference.

Webster, W., 1995. Mooring-induced damping. Ocean Eng. 22 (6), 571–591.

Wichers, J.E.W., Huijsmans, R.H.M., 1990. The contribution of hydrodynamic damping induced by mooring chains on low-frequency vessel motions. In: Offshore Technology Conference.

Xiong, L., Yang, J., Zhao, W., 2016. Dynamics of a taut mooring line accounting for the embedded anchor chains. Ocean Eng. 121, 403–441.

Xiong, L., Yang, J., Lv, H., Zhao, W., Kou, Y., 2016. Study on global performances and mooring-induced damping of A semi-submersible. China Ocean Eng. 3–5, 671–686.

Yang, Y., Chen, J.-X., Huang, S., 2016. Mooring line damping due to low-frequency superimposed with wave-frequency random line top end motion. Ocean Eng. 112, 243–252.